Photonics and Optoelectronics

Digital Optical Neural Networks for Large-scale Machine Learning

L. Bernstein, A. Sludds, R. Hamerly, D. Englund
Sponsorship: NSERC, NSF, NTT, ISN

Artificial intelligence is becoming ubiquitous in our society; specifically, artificial deep neural networks (DNNs) have enabled breakthroughs in image classification, translation and prediction. The recent adoption of DNNs in a wide variety of fields is largely due to algorithms with improved accuracy that leverage more compute power and larger datasets. However, throughput and energy efficiency are currently limiting the further expansion and adoption of DNNs. We have proposed optical neural networks (ONNs), which we have theoretically shown to achieve low-energy, high-throughput DNN processing. Our latest results include a proof-of-concept demonstration of a digital ONN with little drop in classification accuracy on the MNIST dataset (-0.6% on a custom, fully-connected, 3-layer network, due to optical crosstalk). In this scheme, we use optics for passive digital data fan-out and routing. Owing to the length-independence of energy and latency in optical data transmission, we find that the digital ONN may enable more efficient DNN hardware. This work showcases the promise of ONNs as a new computing paradigm, which is required to unlock the full potential of DNNs.

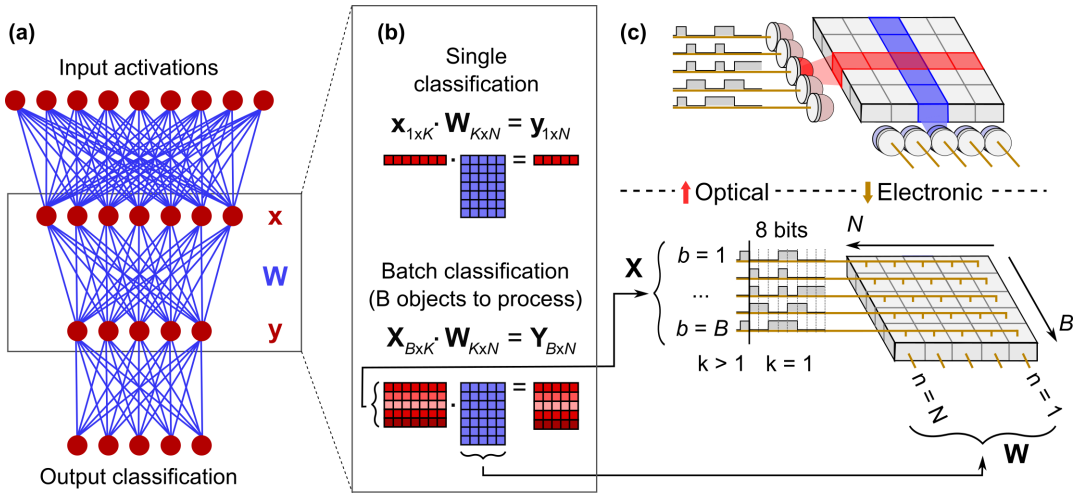

▲Figure 1: (a) Fully-connected neural network (FC-NN). (b) Matrix formulation of FC-NN. (c) Digital optical implementation of FC-NN (top) compared with equivalent monolithic multiplier array (bottom).

Charge-carrier Recombination in Halide Perovskites

D.W. deQuilettes, K. Frohna, D. Emin, T. Kirchartz, V. Bulović, D. S. Ginger, S. D. Stranks
Sponsorship: Tata Trusts

The success of halide perovskites in a host of optoelectronic applications is often attributed to their long photoexcited carrier lifetimes, which has led to charge-carrier recombination processes being described as unique among semiconductors. Here, we integrate recent literature findings to provide a critical assessment of the factors we believe are most likely controlling recombination in the most widely studied halide perovskite systems. We focus on four mechanisms that have been proposed to affect measured charge-carrier recombination lifetimes, namely: (1) recombination via trap states, (2) polaron formation, (3) the indirect nature of the bandgap (e.g., Rashba splitting), and (4) photon recycling (Figure 1). We scrutinize the evidence for each case and the implications of each process for carrier recombination dynamics. Although they have attracted considerable speculation, we conclude that shallow trap states and the possible indirect nature of the bandgap (e.g., Rashba splitting), seem to be less likely given the combined evidence, at least in high-quality samples most relevant to solar cells and light-emitting diodes. On the other hand, photon recycling appears to play a clear role in increasing apparent lifetime for samples with high photoluminescence quantum yields. We conclude that polaron dynamics are intriguing and deserving of further study. We highlight potential interdependencies of these processes and suggest future experiments to better decouple their relative contributions. A more complete understanding of the recombination processes could allow us to rationally tailor the properties of these fascinating semiconductors and will aid the discovery of other materials exhibiting similarly exceptional optoelectronic properties.

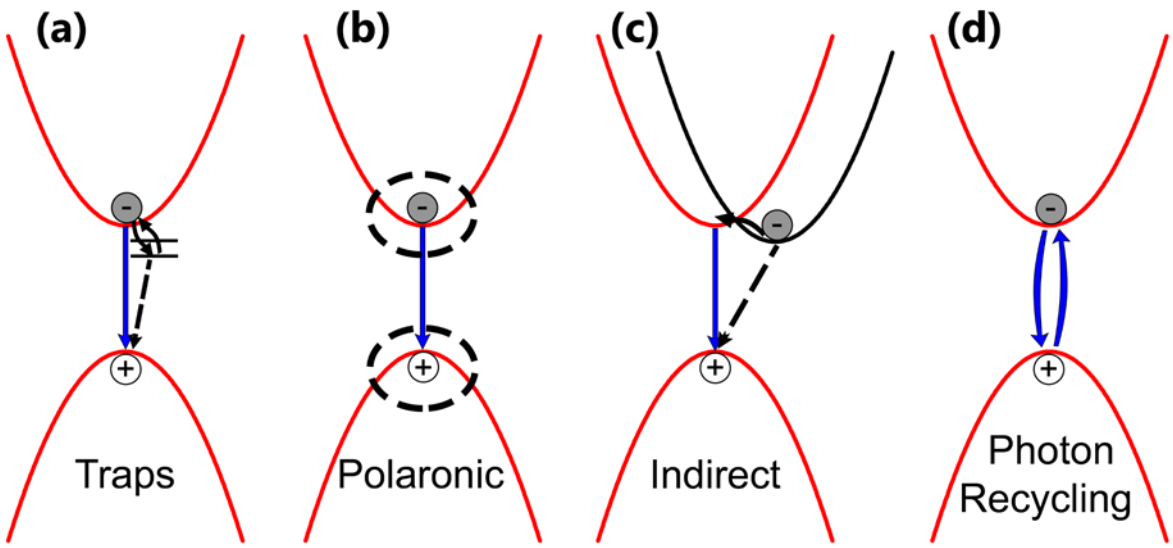

▲ Figure 1: Proposed mechanisms that may impact charge carrier recombination in perovskites: (a) trapping, (b) polaronic effects, (c) indirect bandgap character, and (d) photon recycling.

FURTHER READING

- D. W. deQuilettes, K. Frohna, D. Emin, T. Kirchartz, V. Bulović, D. S. Ginger, S. D. Stranks, "Charge-carrier Recombination in Halide Perovskites," *Chem. Rev.*, vol. 119, no. 20, pp. 11007-11019, 2019.

In-situ Gamma Radiation Damage on SiC Photonic Devices

Q. Du, J. Michon, B. Li, D. Kita, D. Ma, H. Zuo, S. Yu, T. Gu, A. Agarwal, M. Li, J. Hu
Sponsorship: DTRA

In this report, we demonstrate real-time, in-situ analysis of radiation damage in integrated photonic devices. The devices, integrated with an optical fiber array package and a baseline-correction temperature sensor, can be remotely interrogated while exposed to ionizing radiation over a long period without compromising their structural and optical integrity. We also introduce a method to deconvolve the radiation damage responses from different constituent materials in a device. The approach was implemented to quantify gamma radiation damage and post-radiation relaxation behavior of SiO2-cladded SiC photonic devices. Our findings suggest that densification induced by Compton scattering displacement defects is the primary mechanism for the observed index change in SiC. Additionally, post-radiation relaxation in amorphous SiC does not restore the original pre-irradiated structural state of the material. Our results further point to the potential of realizing radiation-hard photonic device designs taking advantage of the opposite signs of radiation-induced index changes in SiC and SiO2.

The devices fabricated following CMOS-compatible protocols are symmetrically cladded with PECVD SiO2. In device packaging, the as-fabricated devices were packaged with optical fiber arrays (SQS Vlaknova Optika) using ultraviolet-curable epoxy (Masterbond UV15TK) as the bonding agent. Fibers with an incident angle of 15° were first active aligned to the on-chip grating couplers to maximize the transmitted power. Epoxy was applied onto the chip to securely bond the fibers to the chip. The active alignment was repeated after epoxy application to ensure optimal coupling. The epoxy was then cured through flood UV exposure. We monitored the device resonance peak position and Q-factor as gamma radiation progressed. The refractive index and absorption coefficient change of a-SiC core and a-SiO2 cladding were extract and plotted in Figure 1. As indicated in the graph, we clearly observe an opposite in signs of index change in these two materials, suggesting the potential of realizing radiation-hard photonic devices.

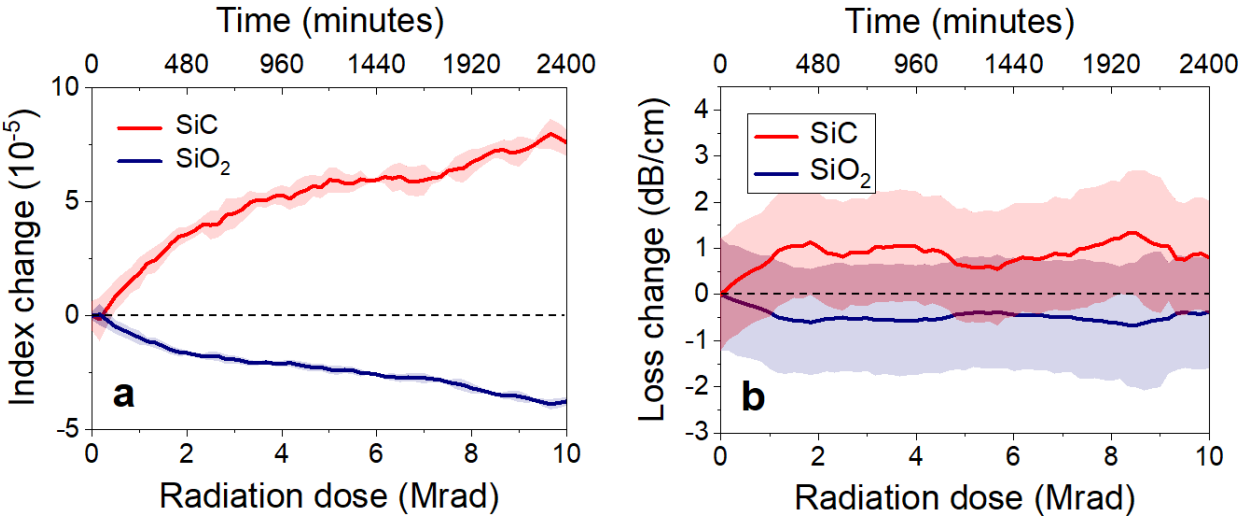

▲ Figure 1: In-situ measured changes of (a) refractive indices and (b) optical losses in SiC and SiO_2 induced by gamma ray irradiation.

FURTHER READING

- Q. Du, J. Michon, B. Li, D. Kita, D. Ma, H. Zuo, S. Yu, T. Gu, A. Agarwal, M. Li, and J. Hu, "Real-time, In-situ Probing of Gamma Radiation Damage with Packaged Integrated Photonic Chips," *Photon. Res.*, vol. 8, no. 2, pp. 186-193.

Variation-aware Compact Models for Yield Prediction of Coupled-resonator Optical Wave-guides

S. I. El-Henawy, D. S. Boning
Sponsorship: AIM Photonics

Silicon photonics is a growing design platform due to all the potential applications and enhancements it can offer. Among these attractive applications are the significant computing system performance gains that can be achieved by transferring information using optical rather than electrical signals. Achieving this optical transmission requires on-chip optical buffers. Coupled resonator optical waveguides (CROWs), which chain a number of ring waveguides together as in Figure 1a, can be used as buffers.

However, CROWs are challenged by the spatial variations within die or across the wafer, as CROWs are large structures extending hundreds of microns to millimeters in length depending on the number of constituent rings. These variations can change the passband or, more importantly, may cause the CROW to fail if the spatial variations cause the resonances of the coupled rings to lose their alignment. Moreover, varying the ring (constituting a CROW) design requires regenerating the S-parameters, which is computationally expensive and time-consuming, if many variants need to be considered for Monte-Carlo statistical simulations or during design optimization. This highlights the need for a variation-aware compact model.

We develop a method and variation-aware compact models that can be used to simulate and predict the CROW behavior (S-parameters) against spatially correlated process variations in thickness and width. Figure 1b compares the simulated performance of a 28-ring CROW using S-parameters generated directly from FDTD simulation and using S-parameters generated using the developed compact model. This parametrized compact-model-generated S-parameters can be used to facilitate and speed up design optimization, run Monte-Carlo simulations, and predict yield. Figure 2 shows the yield prediction of CROWs satisfying a sufficient amplitude pass band (above -20dB), in response to width variation as a function of spatial correlation length ( ) and amplitude (σ). This compact model can serve as a building block for a variation-aware process design kit (PDK) for photonics.

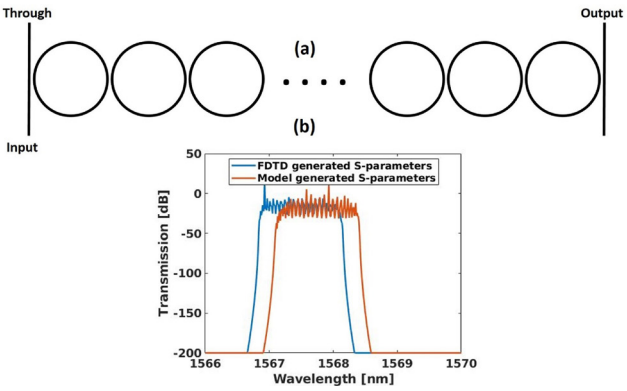

▲Figure 1: a) Schematic of CROWs, b) transmission simulation using variation-aware compact model vs. direct FDTD-based S-parameter model for 28-ring CROW with width = 504 nm and thickness = 220 nm.

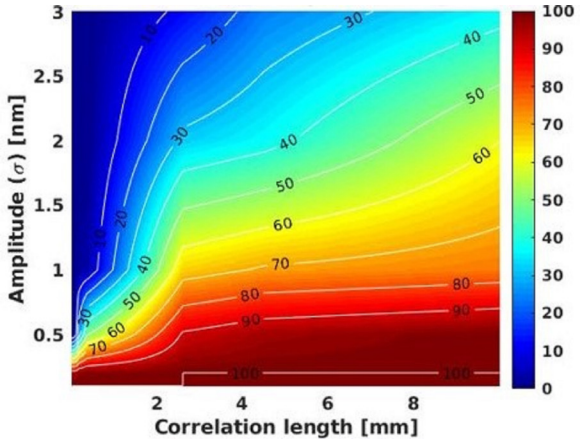

▲Figure 2: Yield (%) vs. spatial length correlation and amplitude of width for 100-ring CROWs.

FURTHER READING

- W. Bogaerts, P. De Heyn, T. Van Vaerenbergh, K. De Vos, S. Kumar Selvaraja, T. Claes, P. Dumon, P. Bienstman, D. Van Thourhout, and R. Baets, "Silicon Microring Resonators," *Laser & Photonics Reviews*, vol. 6, no. 1, pp. 47–73, 2012.
- S. I. El-Henawy, C. Lang, and D. S. Boning, "Yield Prediction for Coupled-resonator Optical Waveguides Using Variation-aware Compact Models," *Frontiers in Optics, Optical Society of America*, pp. FTu1C-3, 2019.

Graphene-loaded Slot Antennas for Multispectral Thermal Imaging

J. A. Goldstein, D. R. Englund
Sponsorship: ARO via ISN-4 Research Grant

Color cameras are ubiquitous in everyday life. However, most color imagers rely on color filter arrays (CFAs), resulting in most incoming light being filtered out instead of detected. More generally, for a filter-based imaging array with N different colors, only 1/N of the incoming light is actually used. While lossless spectral imagers are available, they rely on bulky optics such as diffraction gratings or interferometers to achieve spectral resolution, which is often undesirable. In the thermal IR wavelength range, the problem of filter loss is exacerbated by reduced sensor detectivity compared to visible light sensors. We propose an efficient and compact thermal IR spectral imager based on a metasurface consisting of sub-wavelength-spaced, differently-tuned antennas with photosensitive loads. The different antenna resonances combine to yield broadband optical energy transfer to the loads exceeding the 1/N efficiency limit of CFAs. In particular, we investigate slot antennas due to their unidirectionality and high efficiency compared to typical dipole antennas. We use graphene as our photosensitive load because its 2D nature makes it easily adaptable to this imager architecture. To aid in the design of these slot antenna metasurfaces, we establish a circuit model for the optical properties of the antennas and demonstrate consistency between this model and full-wave electromagnetic simulations. We also show simulations results demonstrating broadband ~36% free space to graphene coupling efficiency for a six-spectral-band metasurface. Finally, we demonstrate a fabrication process which yields slot antennas with smooth surfaces suitable for graphene transfer on top. This research represents the first steps towards compact, monolithic, and potentially CMOS-integratable mid-IR spectral imagers whose low bulk and low energy consumption suit them for deployment on small drones for remote sensing and free-space communication purposes.

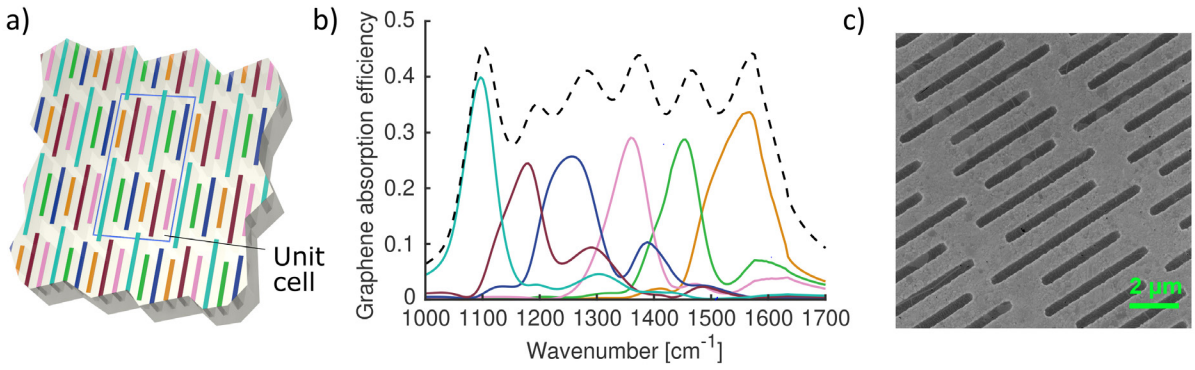

▲ Figure 1: a) Multispectral metasurface absorber, with graphene loads color-coded by center wavelength. b) Incident light to graphene power transfer efficiency spectrum of metasurface. c) SEM of fabricated gold slots with suspended graphene film.

FURTHER READING

- J. A. Goldstein, and D. R. Englund. "Imaging Metasurfaces based on Graphene-loaded Slot Antennas," arXiv preprint arXiv:2004.06777, 2020.

Room-temperature Strong Light-matter Interactions in Hybrid Perovskites

M. Laitz, D. W. deQuilettes, J. Deschamps, K. Nelson, V. Bulovic

State-of-the-art perovskite materials demonstrate photoluminescence quantum efficiencies (PLQE) above 90% due to low non-radiative recombination rates and unparalleled defect tolerance. The optoelectronic properties that have allowed perovskites to emerge as a leading active layer material in high-efficiency thin-film photovoltaics (PVs)–high absorption coefficient, small Stokes shift, high PLQE, solution processability, and chemical tunability – simultaneously situate perovskites to function superbly as a coherent quantum material. In this work, we explore perovskites as a platform for strong light-matter coupling to sustain all-optical operations. Although light is weakly interacting, it is possible to form interacting quasi-particles, called exciton-polaritons, that have characteristics of both light and matter. Traditionally, polaritons have been studied at cryogenic temperatures in all-inorganic semiconducting materials (e.g., GaAs heterostructures). Here, we study the room-temperature formation of exciton-polaritons with large Rabi splittings in semiconductor microcavities, using solution-processed 2D perovskites as self-assembled quasi-quantum well structures (Figure 1). Polariton formation is probed by angle resolved reflectivity and photoluminescence measurements through a k-space imaging setup. Enhanced polariton propagation is explored by microstructuring the microcavity to funnel polaritons generated in smaller cavity length regions to lower confined photon energy regions of longer cavity length. The realization of stable, facilely-fabricated room-temperature exciton-polaritons has the potential to revolutionize a wide range of devices, from PVs to low-threshold lasers to all-optical switches.

Amorphous Silicon Carbide for Nonlinear Integrated Photonics

D. Ma, P. Xing, K. Ooi, J. Choi, L. Kimerling, D. Tan, A. Agarwal
Sponsorship: Defense Threat Reduction Agency Grant No. HDTRA1-13-1-0001

Silicon carbide (SiC) has been actively researched in recent years as a platform for linear and nonlinear photonics due to its large bandgap, large refractive index, low thermo-optic coefficient, excellent mechanical and chemical stability, and large Kerr nonlinearity. We have demonstrated amorphous SiC waveguides with propagation losses as low as 3 dB/cm, which enable their application in integrated photonics. We have demonstrated amorphous SiC ring-resonators on SiO_2 insulator substrate with an intrinsic quality factor as high as 1.6×10^5. The Kerr nonlinearity obtained at 1550-nm wavelength was $4.8\times10^{-14}cm^2/W$, which was the highest value reported in both crystalline and amorphous SiC material, making it a promising platform for CMOS-compatible nonlinear photonics.

The amorphous SiC photonic devices were fabricated in the MIT.nano cleanroom facilities. A plasma-enhanced chemical vapor deposition (PECVD) system using a silane and methane reactive gas mixture was used to deposit an amorphous SiC thin film on a 6-inch Si wafer that had a 3-μm thermal oxide insulating layer. Electron beam lithography was used to pattern the SiC-on-insulator ring resonators. Fluorine chemistry was used to dry etch SiC using reactive ion etching. We characterized the optical properties of the amorphous SiC photonic devices in collaboration with Dr. Peng Xing and Professor Dawn Tan at the Singapore University of Technology and Design (SUTD) and achieved the largest quality factor among all crystalline and amorphous SiC materials tested to date. The Kerr coefficient of the amorphous SiC film was extracted by fitting the nonlinear Schrödinger equation. The Kerr nonlinearity measured in our amorphous SiC is almost one order of magnitude higher than that reported in the literature for crystalline and amorphous SiC. Nonlinear behavior was observed for the first time for a-SiC at the wavelength of 1550 nm, with a high incident pulse peak power.

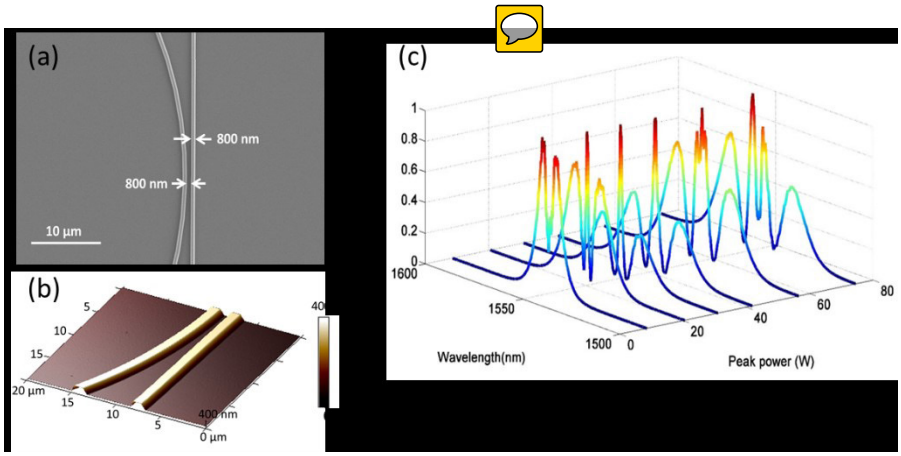

▲ Figure 1: (a) Top view SEM and (b) three-dimensional AFM depth profile of the amorphous SiC ring resonator coupled with a straight waveguide. (c) The measured transmission spectrum of pulses undergoing self-phase modulation at different input peak powers.

FURTHER READING

- D. Ma, Z. Han, Q. Du, J. Hu, L. Kimerling, and A. Agarwal, "DTH Tan, SiC-on-insulator On-chip Photonic Sensor in a Radiative Environment," *IEEE Sensors*, pp. 1-3, 2016.
- P. Xing, D. Ma, K. Ooi, J. Choi, A. Agarwal, and D. Tan, "CMOS Compatible PECVD Silicon Carbide Platform for Linear and Nonlinear Optics," *ACS Photonics*, pp. 1162-1167, 2019.

High Sensitivity Mid-Infrared/Thermal Detectors

E. McVay, Y. Lin, A. Zubair, T. Palacios
Sponsorship: MIT-ARL ISN, NASA NSTRF

Infrared detectors that are fast, high-detectivity, and room-temperature-operable are needed to enable next-generation hyperspectral arrays. While photo conductor (pc) detectors can achieve high detectivity and ~100 ps time constants, pc detectors suffer from a narrow spectral range and must be cooled to cryogenic temperatures for efficient detection beyond ~ 4 μm wavelength. Thermal detectors, meanwhile, exhibit a flat detectivity response with respect to wavelength and can, ideally, reach a detectivity of $1.98*10^{10}$ $cmHz^{1/2}W^{-1}$ at room temperature. In this work we focus on two sensitive novel thermal detector architectures: (1) a nanogap based thermomechanical bolometer and (2) a pyroelectric gated field-effect transistor (FET) biased in the subthreshold regime.

The thermomechanical (thm) bolometer achieves high sensitivity by closing a ~1.3-nm gap as the surrounding materials expand due to infrared light absorption, resulting in an exponential increase in current. The suspended thm bolometer is made of two metal cantilever arms connected by a 5-nm-thick platinum wire (see Figure 1). The nanogap detectors are mechanically stabilized via a self-assembled monolayer (SAM). Early experimental results show temperature coefficient of resistance (TCR) values as high as 0.16 K^{-1}, which is higher than the state-of-the-art ~ 0.1 K^{-1}. Studies to characterize the noise of these devices, measure their response to laser illumination, and determine their detectivity are in progress.

We are also exploring an additional low-power and sensitive bolometer design using subthreshold, pyroelectric gated thin-film transistors. When infrared light is absorbed, dipole charges in the pyroelectric material align and gate the transistor channel. We estimate that these devices can achieve TCR values of $0.6275/I_0$ K^{-1}, where I_0 is the bias current. The proposed device structure can be found in Figure 2. We are currently exploring the design space of $Hf_{0.5}Zr_{0.5}O_2$ ferroelectric/pyroelectric FETs and optimizing them for 5 μm – 10 μm wavelength detection.

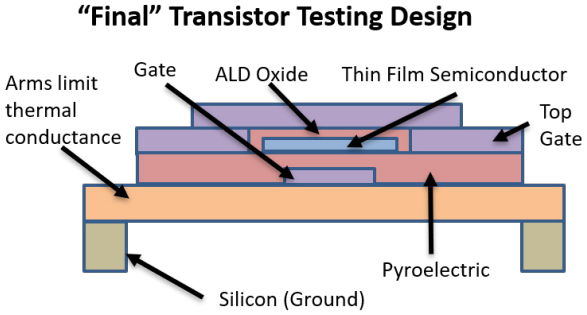

▲ Figure 1: SEM image of suspended thm bolometer.

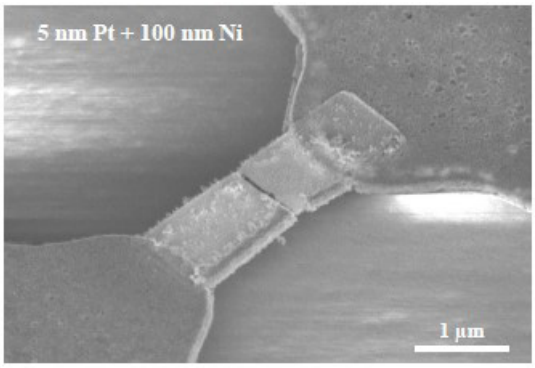

▲ Figure 2: Cross section of proposed pyroelectric gated transistor.

FURTHER READING

- Y. Lin, "Infrared Detectors Based on Two-Dimensional Materials and Heterostructures," Massachusetts Institute of Technology, Cambridge, 2019.

3D Integrated Photonics Platform with Deterministic Geometry Control

J. Michon, S. Geiger, L. Li, C. Gonçalves, H. Lin, K. Richardson, X. Jia, J. Hu
Sponsorship: NSF

3D photonics promises to expand the reach of photonics by enabling both the extension of traditional applications to non-planar geometries and adding novel functionalities that cannot be attained with planar devices. However, current fabrication methods limit the range of available materials options (e.g. to low index contrast polymers for 3D printing) or device geometries (e.g. to curvilinear geometries that are inherently 2D in topology). As an application example, the much-needed ability to monitor stress in biological samples such as cell cultures and tissue models requires a platform that provides precise measurements at multiple, pre-defined locations in 3D, which none of the current fabrication methods for 3D integrated photonics can offer.

In this work, we report a fully-packaged 3D integrated photonics platform with devices placed at arbitrary pre-defined locations in 3D using a fabrication process that capitalizes on the buckling of a 2D pattern. The final structure consists in several buckled strips joining two planar edge platforms, as shown on Figure 1a. Each strip may contain waveguides and waveguide-coupled components such as resonators. We show that our fabricated devices (see Figure 1b) precisely match theoretical shapes. Finally, we demonstrate the amenability of this platform for mechanical strain sensing, e.g. in 3D cell cultures, by calibrating its stress-sensing response. Our results indicate a strain measurement accuracy of 0.01%, for materials with a Young's modulus down to 300 Pa.

A key benefit of our fabrication approach for 3D integrated photonics lies in the wide range of physical and chemical sensing applications of optical resonators, as well as the possibility to multiplex resonators spectrally and spatially. Our platform is thus amenable to monitoring a variety of parameters at a large number of locations in a distributed sensor array, potentially enabling multifunctional sensing, mapping, and light delivery in the 3D space.

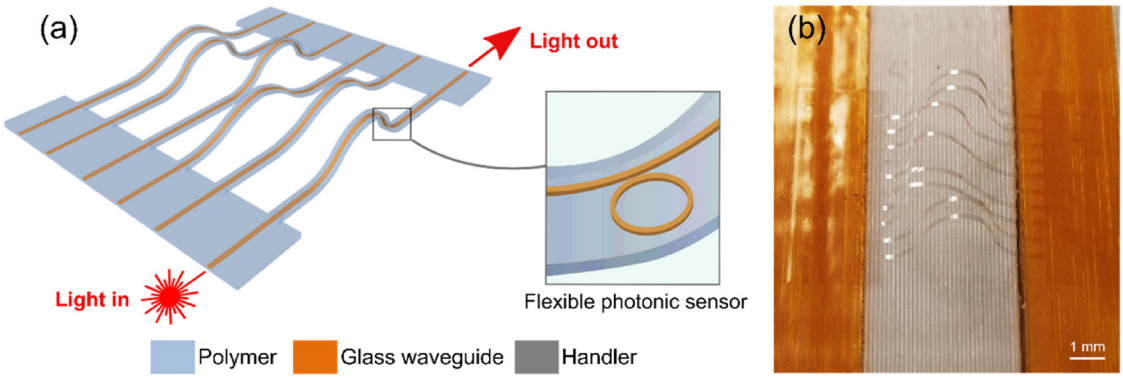

▲ Figure 1: a) Schematic of the 3D device layout. (b) Picture of a fabricated 3D device.

FURTHER READING

- J. Michon, S. Geiger, L. Li, C. Gonçalves, H. Lin, K. Richardson, X. Jia, and J. Hu, "3D Integrated Photonics Platform with Deterministic Geometry Control," *Photonics Research*, vol. 8, pp. 194-201, Feb. 2020.
- L. Li, H. Lin, S. Qiao, Y.-Z. Huang, J.-Y. Li, J. Michon, T. Gu, C. Alonso-Ramos, L. Vivien, A. Yadav, K. Richardson, N. Lu, and J. Hu, "Monolithically Integrated Stretchable Photonics," *Light: Science & Applications*, vol. 7, p. 17138, Feb. 2018.
- L. Li, H. Lin, S. Qiao, Y. Zou, S. Danto, K. Richardson, J. D. Musgraves, N. Lu, and J. Hu, "Integrated Flexible Chalcogenide Glass Photonic Devices," *Nature Photonics*, vol. 8, pp. 643–649, Jun. 2014.

Single-element, Aberration-free Fisheye Metalens

M. Y. Shalaginov, S. An, F. Yang, P. Su, D. Lyzwa, A. Agarwal, H. Zhang, J. Hu, T. Gu
Sponsorship: DARPA EXTREME Program

Wide-angle optical functionality is crucial for implementation of advanced imaging and image projection devices. Conventionally, wide-angle operation is attained with complicated assembly of multiple optical elements. Recent advances in nanophotonics have led to metasurface lenses or metalenses, a new class of ultra-thin planar lenses utilizing subwavelength nanoantennas to gain full control of the phase, amplitude, and/or polarization of light. Here we present a novel metalens design capable of performing diffraction-limited focusing and imaging over an unprecedented > 170° angular field of view (FOV). Similar to a Chevalier landscape lens, our metalens design concept spatially decouples the metasurface and aperture stop, but positions them on a common, planar substrate (Fig. 1a). This optical architecture allows input beams incident at various angles (indicated with colored arrows in Fig. 1a) to be captured on distinct yet overlapping areas of the metasurface. The metasurface further forms the pencil-beams, in such a way, that all of the focal spots are positioned in the same image plane.

We fabricated the metasurface using PbTe meta-atoms of rectangular and H-shaped blocks, which induce distinct phase shifts arising from the electric and magnetic resonant multipole modes (Figure 1b). The meta-atom library consisted of eight elements covering the 360° phase space with a discrete step of 45° for linearly polarized light at the mid-infrared wavelength of 5.2 σm. The implemented metalens produced diffraction limited focal spots when illuminated with a laser beam at the incident angles ranging from 0σ to 85σ. We further demonstrated that the metalens can perform aberration-free imaging of the USAF resolution charts over the entire FOV. Our metalens design concept is generic and can be readily adapted to other meta-atom geometries and wavelength ranges to meet diverse application demands. In the scope of this project, we also explored machine learning approaches to generate free-form metalens designs with improved performance.

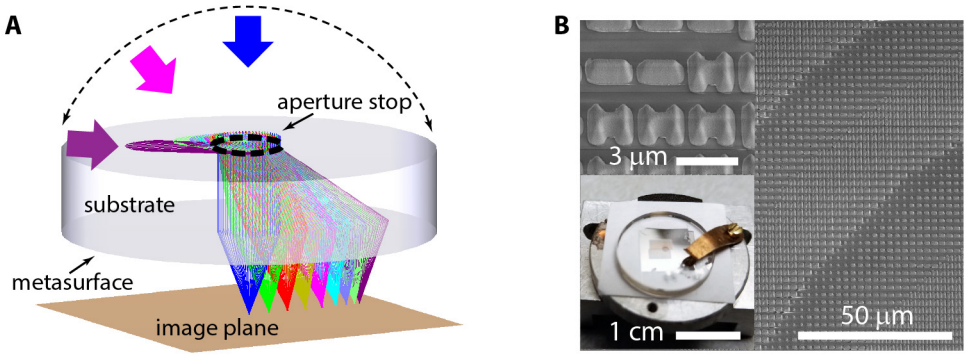

▲ Figure 1: (a) Schematic of 'fisheye' metalens and (b) images of the fabricated metasurface composed of lead telluride (PbTe) nanostructures on a calcium fluoride substrate.

FURTHER READING

- M. Y. Shalaginov, S. An, F. Yang, P. Su, D. Lyzwa, A. Agarwal, H. Zhang, J. Hu, and T. Gu, "A Single-layer Planar Metalens with 170 Degree Field of View", arXiv:1908.2800197.
- L. Zhang, J. Ding, H. Zheng, S. An, H. Lin, B. Zheng, Q. Du, G. Yin, J. Michon, Y. Zhang, Z. Fang, M. Y. Shalaginov, L. Deng, T. Gu, H. Zhang, and J. Hu, "Ultra-thin High-efficiency Mid-infrared Transmissive Huygens Meta-optics," *Nat. Commun.* 9, 1481, 2018.
- P. Lalanne and P. Chavel, "Metalenses at Visible Wavelengths: Past, Present, Perspectives," *Laser Photon. Rev.* 11, 1600295, 2017.

Ultra-sensitive All-optical Membrane Transducers for Photoacoustics

R. Singh, A. Agarwal, B. Anthony

Photoacoustic imaging (PAI) has attracted much attention over the past two decades for various biomedical imaging applications. However, it is surprising to note that this unique imaging modality has not yet spun out much in commercial applications. One of the key obstacles in this direction is the limited sensitivity of the currently available ultrasound transducers. Existing acoustic transducer technologies based on bulk PZT, piezoelectric, and capacitive micromachined ultrasonic transducers have a significantly low sensitivity in orders of 0.2 – 2.0 mPa/sqrt(Hz). This feature limits the imaging depth, reliability, and molecular sensitivity of the current PAI systems.

Our research work explores on-chip CMOS-compatible all-photonic architecture to develop PAI systems with significantly improved sensitivities, improved detection limits, and reduced power consumption. Spiral-shaped silicon nitride waveguides realized on suspended silicon-oxide membranes designed to have a center frequency between 5 MHz to 10 MHz are used as Mach-Zender arms for highly sensitive ultrasound reception with <1 mPa/sqrt(Hz) noise equivalent pressure. Hence, this approach allows fast intensity-based acquisition as opposed to interferometric acquisition, thus allowing on-chip optical interrogation. A few previously reported attempts in this direction have been limited to a single sensor element. Here, we attempt to leverage the benefits of existing photonic-based signal conditioning schemes and adopt them to multiplex the ultrasound reception from multiple sensor elements. The presented transducer technology has a multitude of advantages. Ultra-high sensitivity combined with an all-optical implementation will allow easy scaling-up of the technology and miniaturization for wearable applications.

Large-scale Integration of Diamond Qubits With Photonic Circuits

N. H. Wan, T.-J. Lu, K. Chen, M. Walsh, M. Trusheim, L. De Santis, E. Bersin, I. Harris, S. Mouradian, I. Christen, E. Bielejec, D. Englund
Sponsorship: AFOSR, NSF, ARL

Quantum technologies can potentially offer dramatic speed-up and enhanced security in information processing, communication, and sensing. Such tasks would require the scalable construction and control of a large number of quantum bits (qubits). Here, we report the fabrication and characterization of the largest integrated artificial atom-photonics chip.

Defects such as color centers in diamond behave like "artificial atom" (AA) spin qubits in that they can be controlled via light and microwaves and can maintain long coherence times. Scaling such systems requires (1) high-yield qubit fabrication, (2) efficient photonic wires to route and manipulate single photons, and (3) post-tuning capability to compensate for inhomogeneities between different qubit modules.

Rather than fabricating a low-yield monolithic system with these necessary requirements, we introduced the heterogeneous integration of "quantum micro-chiplets" (QMCs) into an integrated photonics process. The QMC (Figure 1A) consists of AA qubits in a diamond waveguide array, while the photonic integrated circuit (PIC) is an aluminum nitride (AlN)-on-sapphire platform. We used a pick-and-place process to transfer the QMCs in diamond to the AlN photonics chip with success probability over 90% (Figure 1B). As Figure 1C shows, the diamond and AlN modules meet at tapered waveguide interfaces for efficient photon routing from the diamond layer to the integrated photonics layer.

Room temperature and cryogenic measurements reveal single-photon emission in all 128 integrated waveguide channels (Figure 2). Additionally, the emitters exhibit near-lifetime-limited linewidths, indicating high optical coherence of emitters in nanostructures. Finally, we demonstrated on-chip tuning of the qubit optical transitions via strain fields in the waveguide. Our platform paves the way for on-chip generation and manipulation of large entangled quantum states and demonstrates the scalability of optically active spin qubits in solids for quantum information processing.

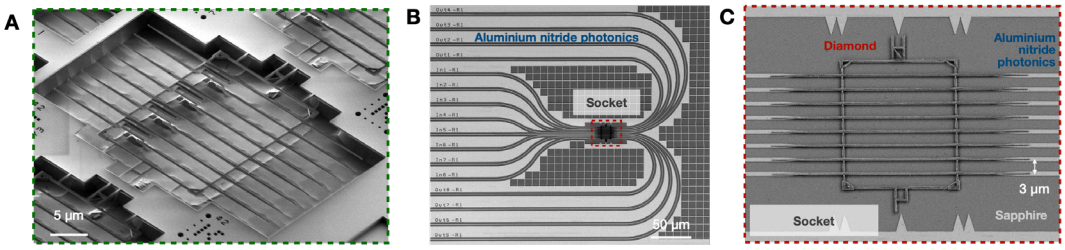

▲Figure 1: (A) Diamond waveguide arrays containing artificial atom spin qubits. (B) A diamond QMC integrated with an aluminum nitride (AlN) photonics platform. (C) Close-up SEM image of the diamond-AlN photonic interfaces.

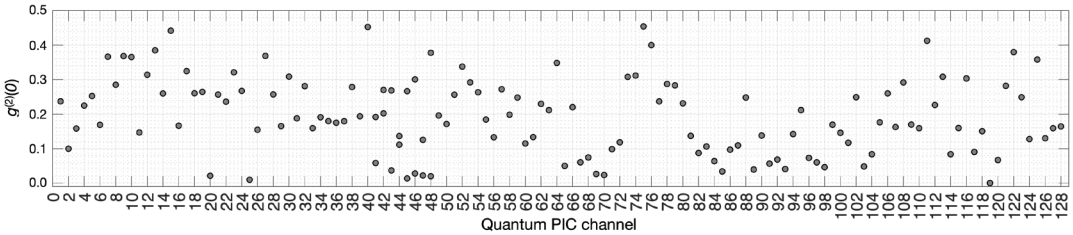

▲Figure 2: Photon intensity autocorrelation measurements confirm single-photon emission and single emitters in all 128 PIC channels.

FURTHER READING

- N. H. Wan, T.-J. Lu, K. C. Chen, M. P. Walsh, M. E. Trusheim, L. De Santis, E. A. Bersin, I. B. Harris, S. L. Mouradian, I. Christen, E. S. Bielejec, and D. Englund, "Large-scale Integration of Artificial Atoms in Hybrid Photonic Circuits," *Nature 583*, 226-231, 2020.

Transmittance Enhancement at Graphene/Al Interfaces

H. Wang, S. Fu, J. Liu, J. Kong

When two metal films stack together forming "hetero-film," it has been generally accepted that the effective transparency is lower than in the respective metal film as a result of the absorption accumulation. In this work, we investigated the counterintuitive transmittance enhancement of graphene/aluminum hetero-films. Single layer graphene was first grown by chemical vapor deposition and transferred on SiO2 substrate. Subsequently, an aluminum coating with a thickness of 4-20 nm was produced by an e-beam evaporator with a target of 99.99% pure aluminum. We acquired the transmittance spectra of graphene/aluminum hetero-films using a UV-vis-NIR spectrophotometer. One interesting observation is that transmittance increased in samples with graphene, indicating a novel physical or chemical interaction between graphene and aluminum. For 4-nm Al film, graphene induced transparency enhancement at UV range of 200 to 300 nm. As film thickness increases to 8 nm, the transparency enhancement extends to a wider UV range of 10-660 nm. In a 12-nm sample, we observe an averaged 12% increase in transmittance for the wavelength range of 500-2500 nm in the sample with graphene, compared with a pure Al coating on the substrate. More surprisingly, similar transparency enhancement is captured when Al film was deposited on the graphene film. Due to the counterintuitive observation, we anticipate this work will benefit the community in fundamental understanding and reliable utilization of graphene and Al interactions.

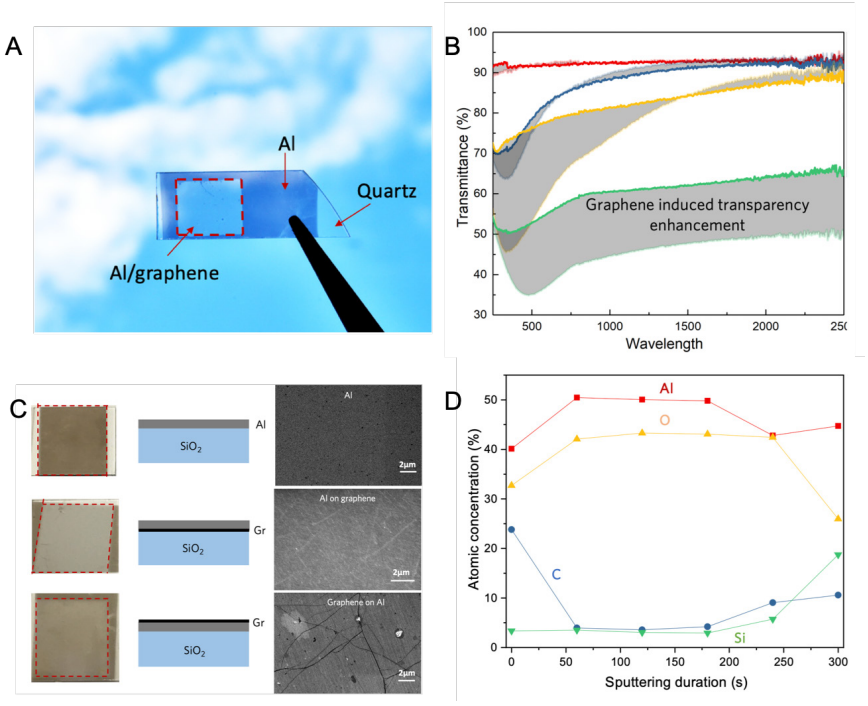

▲Figure 1: (A) Image to show the transmittance enhancement at Al/graphene interface; (B) Transmittance in the samples with and without graphene; (C) Surface morphologies of Al/SiO2, Al/Gr/SiO2 and Gr/Al/SiO2 samples; (D) XPS depth-profile of Al/Gr/SiO2 sample.

FURTHER READING

- H. Wang, et al. "Optical Properties of Graphene/Al Hetero-film." *APS Meeting Abstracts*. 2019.2.
- S. Fu, et al. "Self-assembled, Ultrahigh Refractive Index Pseudo-periodic Sn Nanostructures for Broad-band Infrared Photon Management in Single Layer Graphene." *ACS Photonics* 6.1 (2018): 50-58

Decomposed Representation of S-Parameters for Analysis of Silicon Photonic Variation

Z. Zhang, S. I. El-Henawy, D. S. Boning
Sponsorship: AIM Photonics

Silicon photonics offers great potential for monolithic integrated photonic and electronic components using existing integrated circuit (IC) fabrication infrastructure. However, methods to analyze the impact of IC process variations on performance of photonic components remain limited.

Statistical models based on either simulations or experiments that quantify the effect of these variations are necessary to achieve high-yield manufacturing. To cope with the non-linearity in the S-parameters of photonic device components and circuits, non-linear parameter fitting is often used prior to statistical modeling, e.g., rational polynomial fitting of ring resonator responses. The traditional approach treats the amplitude and phase of the S-parameters separately in the fitting process; however, this method can be problematic when the behavior of the S-parameters becomes complicated under the variations since it neglects the strong correlation between amplitude and phase. For example, the seemingly complicated spike in group delay shown in Figure 1 is actually where a smooth S-parameter accidentally crosses the origin point.

We present a novel representation of S-parameters that decomposes the complex-numbered S-parameters into several components, each having a simple response that does not require non-linear parameter fitting and that supports subsequent statistical analysis. We apply the proposed S-parameter decomposition method to Y-splitters with imposed line edge roughness (LER) variations. In contrast to the difficulty of the traditional amplitude-phase representation, the decomposed representation shows improvement in statistical modeling of variation ensembles, e.g., using principle component analysis (PCA) (Figure 2).

The method can be extended to other photonic components and circuits with other process variations to help quantify the effect of process variations for statistical analysis and to help designers predict and optimize photonic component performance and yield.

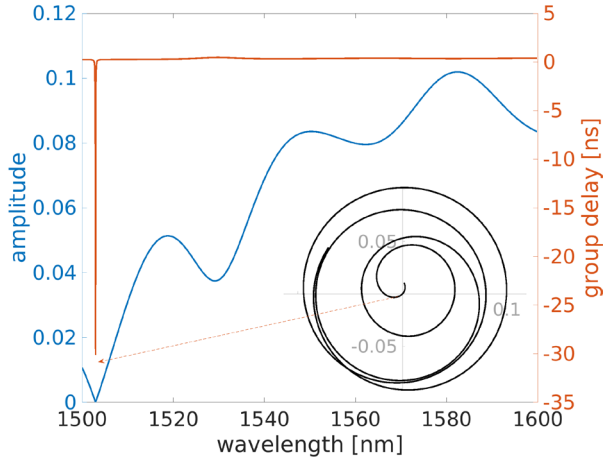

▲Figure 1: Typical back-reflection S-parameter of a Y-splitter with LER. Although the amplitude (blue solid) and phase (red solid) responses look complicated to model, the actual S-parameter trajectory in the complex plane (inset figure) is relatively smooth and simple.

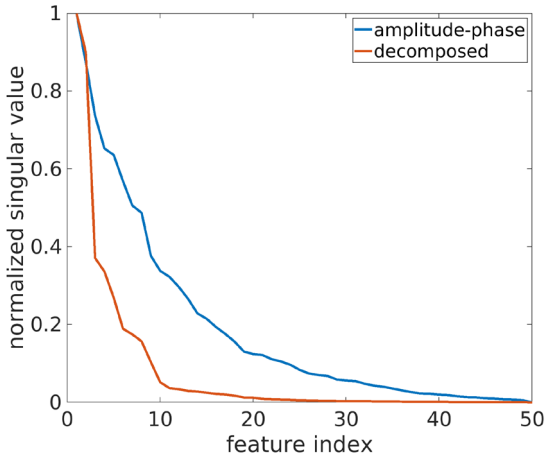

▲Figure 2: Results of applying PCA on the back-reflection S-parameter of a Y-splitter ensemble with LER based on the original amplitude-phase representation (blue) and the proposed decomposed representation (red).

FURTHER READING

- L. Chrostowski and M. Hochberg, "Silicon Photonics Design: from Devices to Systems," Cambridge: *Cambridge University Press*, 2015.
- T.-W. Weng, Z. Zhang, Z. Su, Y. Marzouk, A. Melloni, and L. Daniel, "Uncertainty Quantification of Silicon Photonic Devices with Correlated and Non-Gaussian Random Parameters," *Opt. Express* vol. 23, pp. 4242-4254, 2015.